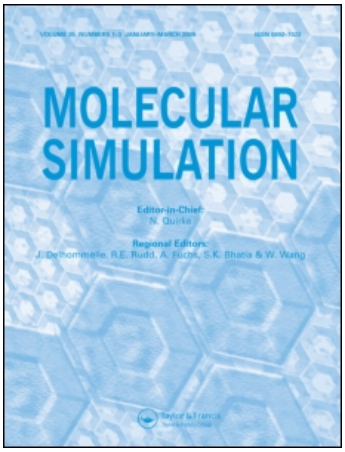

Molecular Simulation
Publication details, including instructions for authors and subscription information:
http://www.informaworld.com/smpp/title~content=t713644482

Dynamical Studies of Translational and Rotational Hindrance of A Needle Fluid in Random Porous Media

K. Raghavan[a]; J. M. D. Macelroy[a]
[a] Department of Chemical Engineering, University of Missouri-Rolla, Missouri, USA

To cite this Article Raghavan, K. and Macelroy, J. M. D.(1991) 'Dynamical Studies of Translational and Rotational Hindrance of A Needle Fluid in Random Porous Media', Molecular Simulation, 8: 1, 93 — 117
To link to this Article: DOI: 10.1080/08927029108022469
URL: http://dx.doi.org/10.1080/08927029108022469

Molecular Simulation, 1991, Vol. 8, pp. 93–117
Reprints available directly from the publisher
Photocopying permitted by license only

DYNAMICAL STUDIES OF TRANSLATIONAL AND ROTATIONAL HINDRANCE OF A NEEDLE FLUID IN RANDOM POROUS MEDIA

K. RAGHAVAN and J.M.D. MACELROY

Department of Chemical Engineering, 143 Schrenk Hall, University of Missouri-Rolla, Rolla, Missouri 65401, USA

(*Received December 1990, accepted March 1991*)

A major computational difficulty in hard-body molecular dynamics (MD) simulations is the possibility of root bypassing in the collision algorithm. In this paper we report MD simulation results for a system which is significantly affected by this problem, namely hard needle particles confined within the void space of random two-phase models of porous media. In the case of very long needles, high radial velocities preclude the use of moderately large time steps in the trajectory calculations. Conventional Newton–Raphson methods are known to be deficient in detecting all roots in the collision analysis and here we introduce a novel technique based on homotopy continuation as our root-finding algorithm. This method is a highly robust technique for the detection of all possible roots in the collision sequence for this type of system.

The needle particle/model porous medium, in which the latter is represented as an assembly of solid spheres randomly distributed in space, is an idealization of a confined rigid polymer fluid. One of the objectives in these studies has been to examine the effects of the porosity of the medium and the length of the needles on the transport properties of this system. In particular, the transition from free to hindered rotation as the needle length is increased and its influence on the translational dynamics of the particles are investigated. The results obtained suggest that rigid linear molecular structures may experience significantly enhanced diffusion rates in micropores as a consequence of alignment parallel to the solid surface within the porous medium.

KEY WORDS: Diffusion, percolation, needle fluid, hindered rotation, micropores.

1 INTRODUCTION

Hard-body dynamical simulations were pioneered by Alder and Wainwright [1] for homogeneous hard sphere and square-well fluids nearly four decades ago. Since then interest in simulating other classes of hard core particles such as ellipsoids [2], spherocylinders [3], needles [4–7] and composite sphere models [8], has rapidly grown. These studies have been primarily motivated by the desire to develop accurate results for hard-body reference fluids in perturbation theories of equilibrium statistical mechanics and also to provide insight into the influence of particle asphericity on the transport properties of molecular systems.

In recent years technological developments in solid/fluid separation processes and heterogeneous catalysis have also stimulated interest in confined systems and particularly in micropore fluids. These solid/fluid systems are influenced both by the fluid particle size and shape as well as the topology of the microporous medium. Studies in this area have usually been directed along either one of two possible avenues of inquiry, (i) an investigation of the behaviour of simple fluids of structureless particles confined within two phase random models of microporous media or (ii) determination

of the properties of different particulate fluids in pores of idealized geometry. The configurational and dynamical properties of hard sphere fluids confined within complex pore structures generated by randomly distributed inclusions such as spheres [9] or fibers [10] and randomly distributed holes [11] have been investigated. Of particular interest in these studies was the continuum percolation behaviour of fluids in random media and it was primarily for this reason that simple structureless fluid particles were employed in the simulations. In a number of recent articles, however, [12, 13] the influence of particle structure as well as size has also been addressed, although in these studies the pore models employed were of comparatively simple shape. Furthermore, the simulations reported in [12, 13] were primarily concerned with equilibrium rather than nonequilibrium pore fluid properties and, to our knowledge, the only simulation results available at present on the dynamical properties of inhomogeneous aspherical fluids are those reported by Magda *et al.* [14] for a needle fluid confined within slit-shaped pores and by Bitsanis *et al.* [15] for models of polymer melts confined between two hard walls.

In this paper we extend our earlier work on dilute hard sphere fluids [9] to an investigation of the dynamics of a needle fluid in a random two phase model of a microporous medium. This fluid model is of sufficient simplicity to permit a detailed analysis of its properties and it is employed here primarily to investigate the coupling of translational and rotational modes of motion in micropores as well as the influence of the porous structure on the particle dynamics. Simulations of needle or rod fluids are however not as straightforward as they might first appear. This is demonstrated, for example, in the work of Sando and Rebertus [3] for a bulk system of spherocylindrical hard core particles in which an *a posteriori* overlap criterion was employed to detect collisions. This technique, which is based on Newton's first order algorithm, is subject to the possibility of improper trajectory analysis due to collision bypassing. This problem is further emphasized in the work of Frenkel and Maguire [4] who found it necessary to develop a new *a priori* technique to detect collisions in a needle fluid. Their method was derived from a second order Newton–Raphson procedure and is unique for simulations of that type. The problem of collision bypassing is also particularly acute when the needle undergoes highly restricted motion within a confined space and a primary objective of the studies reported here was to develop a new algorithm for this purpose.

In Section 2 the simulation procedures for investigating the dynamics of a dilute needle fluid using a novel collision tracking technique are described. This procedure, which is known as Newton Homotopy Continuation (NHC), is not subject to the shortcomings of the Newton–Raphson (NR) first order method and the ability of NHC in this regard is demonstrated in Section 3. Results obtained for a wide range of needle lengths and porosities are also presented in Section 3 and the transition from free to hindered motion is examined in detail. Finally in Section 4 we summarize the most important conclusions of this work.

2 MODELS AND SIMULATION TECHNIQUES

Molecular dynamics simulations of a dilute needle fluid diffusing in a random overlapping two-phase model of a microporous medium were conducted in these studies. Figure 1 illustrates the model for the pore structure of the medium which is generated by a system of randomly distributed overlapping solid spheres. The porosity, ψ, of this

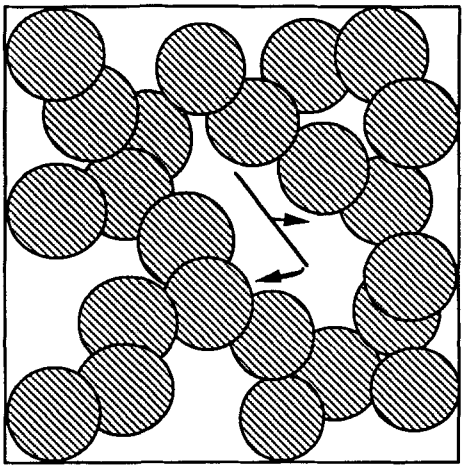

Figure 1 The random overlapping spheres model and the confined needle fluid.

medium is given by [16]

$$\psi = \exp(-\tfrac{4}{3}\pi n_s \sigma^3) \tag{1}$$

where n_s is the number density of the solid spheres of radius σ. The dilute needle fluid confined within the micropores is chosen to be a single particle undergoing free molecule diffusion within the pore space. The needle is an infinitely thin rod with its moment of inertia I given by

$$I = \frac{L^{*2}}{12}$$

where I is in units of $m\sigma^2$. The needle length L^* is reduced by σ and, as implied in the above expression, the mass, m, of the needle is considered to be uniformly distributed along its length.

In contrast to homogeneous bulk needle fluid simulations, where all the collisions are of a single type, the needle in the random medium shown in Figure 1 may undergo two different modes of collision: (i) a glancing collision or (ii) a head-on or tip collision. These two types of collisions are also present in needle fluids confined within a slit pore [14] although they do not occur for the same collision pairs, i.e. glancing collisions are only possible between needle particles, while needle-wall collisions are strictly tip overlaps. The latter is true for all pore models having concave surfaces, however in our case the solid structure has a convex surface and needle-wall collisions can be of either type. The nature of the convex surface enhances the possibility of collision bypassing and therefore the dynamics cannot be reliably handled by traditional Newton methods. For this reason we employ a new approach known as Newton Homotopy Continuation (NHC) to determine the collision sequence in the trajectory.

Homotopy continuation methods have been in use for twenty years as efficient techniques for the evaluation of all possible roots for systems of non-linear algebraic

equations described by smooth, continuous vector functions of the type

$$\mathbf{f}(\mathbf{x}) = \mathbf{0}$$

In our case with only one independent parameter, i.e. time, the vector function $\mathbf{f}(\mathbf{x})$ is replaced by a scalar $f(t)$. The homotopy path, which is central to the determination of the roots of $f(t) = 0$, is described by a function $h(t,\tau)$ given by

$$h(t,\tau) = \tau f(t) + (1 - \tau)g(t) = 0 \tag{2}$$

where τ is known as the homotopy parameter and $g(t)$ is some other known function. This technique converges on the solution by tracing the curve from $\tau = 0$ to $\tau = 1$. At $\tau = 0$, the starting point $t = t_0$ is the solution to the function $g(t) = 0$ and the path, when traced to $\tau = 1$, yields the solution to the function $f(t) = 0$. Equation (2) is a general form for linear convex homotopies and the Newton Homotopy is derived by replacing the function $g(t)$ by $f(t) - f(t_0)$, i.e.

$$h(t, \tau) = \tau f(t) + (1 - \tau)(f(t) - f(t_0)) = 0 \tag{3}$$

In our studies, the function $f(t)$ is the square of the relative separation between the points of closest approach on the needle and on a given sphere within the system.

The NHC method is only one of a number of possible homotopy techniques (see for example [17], [18]) and was chosen here as our root-finding procedure for the following reasons:

(i) NHC detects all possible roots for a single dimension function if the homotopy function is tracked to infinity;

(ii) The homotopy function $h(t, \tau)$ for NHC is only dependent on the function $f(t)$ and the starting point t_0. Hence the path coincides with the function $f(t)$ itself and therefore ensures that the solution to $h(t, \tau) = 0$ at $\tau = 1$ is also the solution to $f(t) = 0$.

The path in NHC needs to be tracked in both the positive and negative τ directions and Figure 2 illustrates the various possible paths that may arise from one starting point on the $\tau = 0$ hyperplane. There are no acceptable roots for paths 1 and 4 since the homotopy either diverges to infinity (path 1) or yields a root on the negative t axis (path 4). The other two paths in this figure illustrate that homotopies may also be traced in opposite directions and yet intersect the $\tau = 1$ hyperplane in the positive t domain. If there are two or more possible roots to the function from the same starting value, the homotopy path, after detecting the first root, proceeds to a turning point and then returns to the $\tau = 1$ hyperplane yielding another root. Additional roots, if any, may be obtained on continuation of the homotopy path.

In view of the linearity of $h(t, \tau)$ there cannot be two values of τ for a single value of t and hence the homotopy path is monotonic in its variations with respect to t. Details on the homotopy path tracking and stopping rules are provided in the Appendix. The path tracking algorithm for the homotopy continuation method was developed by Choi [19] and has been adapted here with relevant modifications which are also described in the Appendix.

NHC was used in conjunction with the free particle equations of motion of a single needle particle to compute its trajectory in random media of the type illustrated in Figure 1. The dynamical properties evaluated from these trajectory calculations included the autocorrelation functions for both the center of mass velocity, $\mathbf{v}$, and

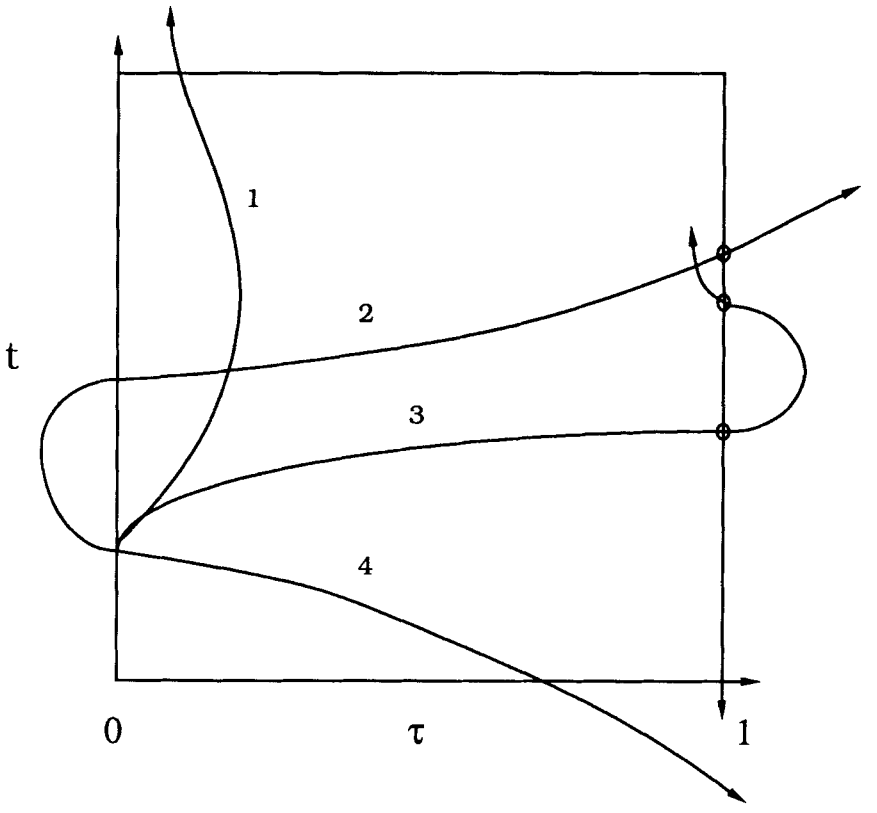

Figure 2 The different homotopy paths which can originate from an arbitrary starting point. The open circles are the roots of the function when the path intersects the hyperplane $\tau = 1$.

angular velocity, ω, which are defined respectively as

$$C_m(t^*) = \langle \mathbf{v}(0) \cdot \mathbf{v}(t^*) \rangle / \langle \mathrm{v}^2 \rangle \tag{4}$$

$$C_\omega(t^*) = \langle \boldsymbol{\omega}(0) \cdot \boldsymbol{\omega}(t^*) \rangle / \langle \omega^2 \rangle \tag{5}$$

where t^* is the reduced time in units of $\sigma/\sqrt{kT/m}$. Furthermore, in order to detect any orientational bias in the diffusion characteristics of the particle undergoing highly restricted motion within the micropores, we computed two other correlation functions for the components of the center of mass velocity parallel and perpendicular to the axis of the needle. These functions are defined by

$$C_\parallel(t^*) = \langle (\mathbf{v}(0) \cdot \mathbf{u}(0))(\mathbf{v}(t^*) \cdot \mathbf{u}(0)) \rangle / \langle \mathrm{v}^2 \rangle \tag{6}$$

$$C_\perp(t^*) = \tfrac{1}{2} \langle (\mathbf{v}(0) \cdot \mathbf{e}_\theta(0))(\mathbf{v}(t^*) \cdot \mathbf{e}_\theta(0)) + (\mathbf{v}(0) \cdot \mathbf{e}_\varphi(0))(\mathbf{v}(t^*) \cdot \mathbf{e}_\varphi(0)) \rangle / \langle \mathrm{v}^2 \rangle \tag{7}$$

where $C_\parallel$ is the time-correlation function of the velocity parallel to the initial orientation of the needle and $C_\perp$ is the corresponding function for motion perpendicular to its axis. In addition to these properties, we also determined C_u, which is the time-correlation function of the velocity along the axis of the needle

$$C_u(t^*) = \langle (\mathbf{v}(0) \cdot \mathbf{u}(0))(\mathbf{v}(t^*) \cdot \mathbf{u}(t^*)) \rangle / \langle \mathrm{v}^2 \rangle \tag{8}$$

The vector **u** in Equations (6) and (8) is the unit vector along the needle while the unit vectors $\mathbf{e}_\theta$ and $\mathbf{e}_\varphi$ in Equation (7) are those perpendicular to it. The correlation functions $C_\parallel$, $C_\perp$ and C_u provide information regarding the directional preference of the diffusing particle as well as the extent of rotational hindrance encountered as a consequence of its size and confinement.

These time-correlation functions were used to determine diffusion coefficients by integration. In particular the center of mass and the angular velocity autocorrelations on integration yielded the translational diffusion coefficient, D_m^* in units of $\sigma\sqrt{kT/m}$ and the rotational diffusion coefficient, D_R^* in units of $\sqrt{kT/m}/(\sigma I)$, respectively. The Green–Kubo relation for both types of diffusion is given by

$$D^* = \lim_{t^* \to \infty} \frac{1}{n_f} \int_0^{t^*} C(\tau^*)\, \mathrm{d}\tau^* \tag{9}$$

where n_f is the number of degrees of freedom available for the type of motion; for translation $n_f = 3$ while for rotation $n_f = 2$. D_m^* was also determined from the average mean square displacements using the Einstein equation [20]

$$D_m^* = \frac{1}{6} \lim_{t^* \to \infty} \frac{\mathrm{d}}{\mathrm{d}t^*} \langle (\mathbf{r}^*(t^*) - \mathbf{r}^*(0))^2 \rangle \tag{10}$$

where $\mathbf{r}^*(t^*)$ is the coordinate of the center of mass of the needle at time t^* in units of σ.

In addition to the dynamical properties described above, we have also evaluated the radial distribution functions for the center of mass and for the tips of the needle with respect to the randomly dispersed solid spheres in the medium. These radial distribution functions are useful measures for detecting possible alignment of the needle parallel to the solid surface. Furthermore, as a consequence of its length, the needle may undergo complete rotational hindrance while diffusing through the micropores. The transition point at which this occurs is generally difficult to determine for a random medium and to gain some insight into the conditions which are responsible for rotational jamming, we have evaluated the free rotational frequency ν_R defined by

$$\langle \nu_R \rangle = \left\langle \left\langle I\left(\omega(t^*)\, \frac{t_c^*}{\pi}\right) \right\rangle \right\rangle \langle \nu_C \rangle \tag{11}$$

where $I(\omega(t^*)t_c^*/\pi)$ is the integral number of times the particle rotates through π radians between two consecutive collisions, $\langle \nu_c \rangle$ is the average collision frequency, $\omega(t^*)$ is the angular velocity of the needle, and t_c^* is the time between two consecutive collisions. The multiple angular brackets in Equation (11) refer to averaging over both the total number of collisions as well as all configurations. Moreover, since the modes of collision of the needle influence its transport, the frequency of occurrence of tip relative to glancing collisions was also recorded.

3 RESULTS AND DISCUSSION

3.1 Comparison of Newton's Method and NHC

To demonstrate the quality of the NHC technique as a root-finding algorithm, preliminary studies were conducted in which both this technique and the Newton–Raphson first order method were independently used to compute trajectories in a

Table 1 System Characteristics for Comparison of the NR and NHC Techniques.

[a]L^*	[b]Δt_N^*	[c]$\nu_c(NR)/\nu_c(NHC)$
1.0	0.005	0.94(2)
	0.0025	0.94(2)
	0.00125	0.95(1)
2.0	0.005	0.94(2)
	0.0025	0.95(1)
	0.00125	0.96(2)

[a] L^* is the needle length in units of the solid sphere radius σ.
[b] Δt_N^* is the timestep used in the Newton–Raphson scheme and is in units of $\sigma\sqrt{m/kT}$.
[c] $\nu_c(NR)/\nu_c(NHC)$ is the ratio of the collision frequencies obtained from the NR and NHC methods respectively. The collision frequencies obtained from NHC for $L^* = 1.0$ and 2.0 are $\nu_c(NHC) = 6.31(7)$ and 8.04(9) respectively in units of $\sqrt{kT/m}/\sigma$.
These simulations were conducted at a porosity $\psi = 0.15$ and the random medium contained 400 solid spheres in each configuration. The total time for the trajectory involved in each configuration was 250 and a statistical sample of 300 configurations was used to compute the results.

number of test cases. In contrast to NHC which, as described in the Appendix, is an *a priori* collision tracking algorithm, the NR method is an *a posteriori* procedure and therefore requires discretization of the trajectory by the use of time steps [2, 3]. In Table 1 we outline the conditions investigated in these test runs. Also shown in this table are the collision frequencies evaluated during the simulations and it is observed that, even though we have emphasized the problem of collision bypassing associated with the NR technique, the collision frequencies obtained using both approaches appear to be in good agreement. However, a significant feature of the results in all cases is that the collision frequencies are lower for the NR procedure and this difference has serious consequences with regard to the dynamical properties of the needle fluid as illustrated in Figure 3.

The velocity autocorrelation functions (VACFs) for the center of mass of the needle shown in Figure 3, clearly demonstrate a serious failing in the NR method. The minima in the VACFs determined by the NR technique are shallower than the corresponding minimum observed in the VACF computed using NHC. Furthermore, the NR correlation functions are shifted to longer times and we associate this effect with an apparent dynamism in the assembly of stationary spheres arising from momentary "appearances" and "disappearances" of the solid spheres as the needle diffuses through the medium. The inset in Figure 3 illustrates the VACFs in the vicinity of the minimum and clearly shows the discrepancy in the results obtained from the two methods.

On integration, the VACFs obtained from the NR and NHC techniques yield the translational diffusion coefficients D_N^* and D_H^* respectively and their ratio is plotted in Figure 4 as a function of the time step Δt_N^* used in the NR method. The results shown in this figure were obtained for two different needle lengths $L^* = 1.0$ and $L^* = 2.0$ at a porosity $\psi = 0.15$. It is observed that the diffusion coefficient D_N^* predicted by the NR procedure is poorer for the larger needle size and the time step required to improve the accuracy of the NR method needs to be smaller the longer the needle. Furthermore, results obtained for a needle length $L^* = 3.0$ and which are not shown here, also demonstrate the failure of the NR procedure at or near a percolation transition. In this case, the NR technique predicts a nonzero diffusion coefficient ($D_N^* = 0.0225$ for $\Delta t_N^* = 0.00125$) while NHC indicates that the particle is localized (nonpercolating) within the medium. This was found to be true regardless

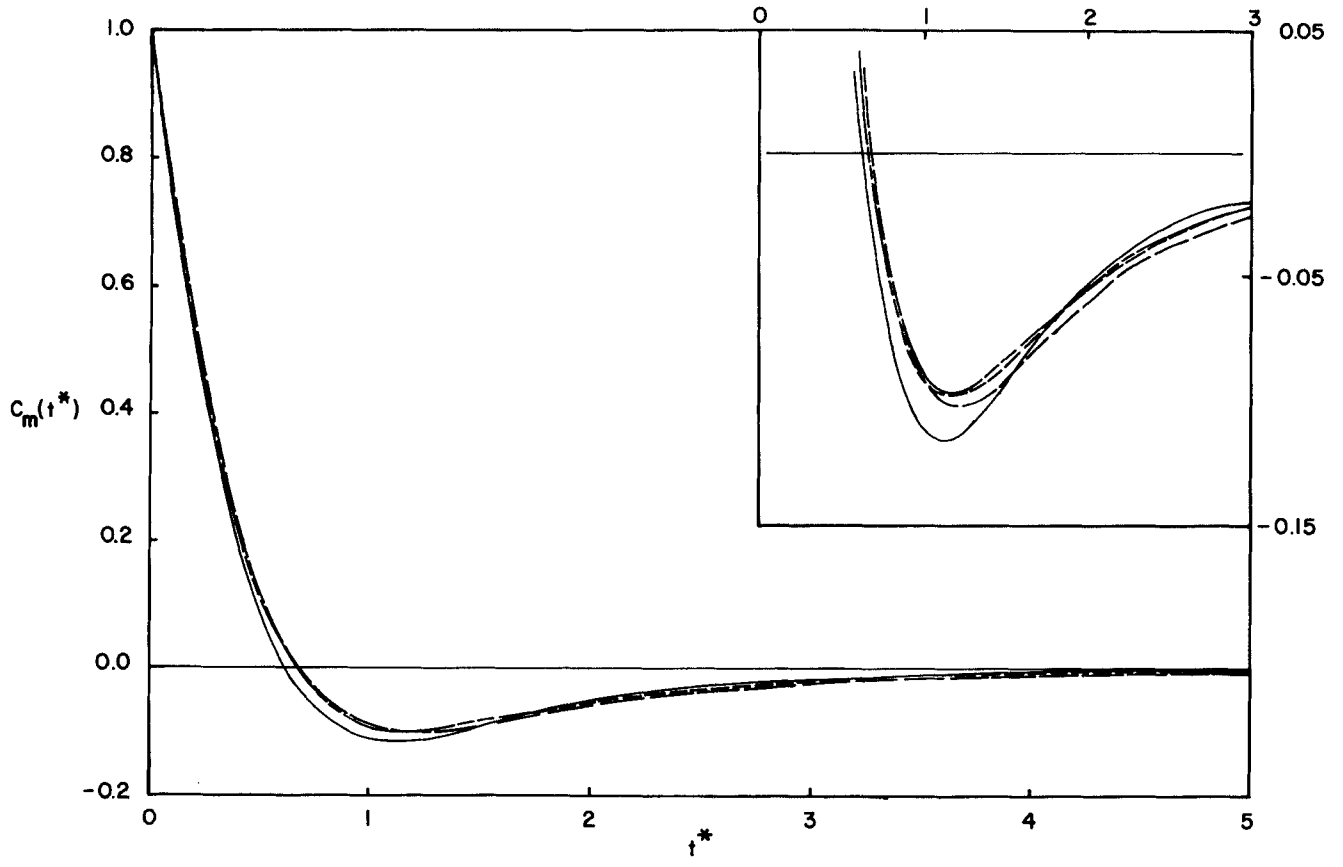

Figure 3 The VACFs obtained from Newton Homotopy Continuation and three different time steps for the first order Newton method. Newton Homotopy Continuation ——; The first order Newton method: - - - - $\Delta t = 0.005$; — - - - $\Delta t = 0.0025$; —— $\Delta t = 0.00125$. The inset shows the region of the minimum in the VACFs for the different cases.

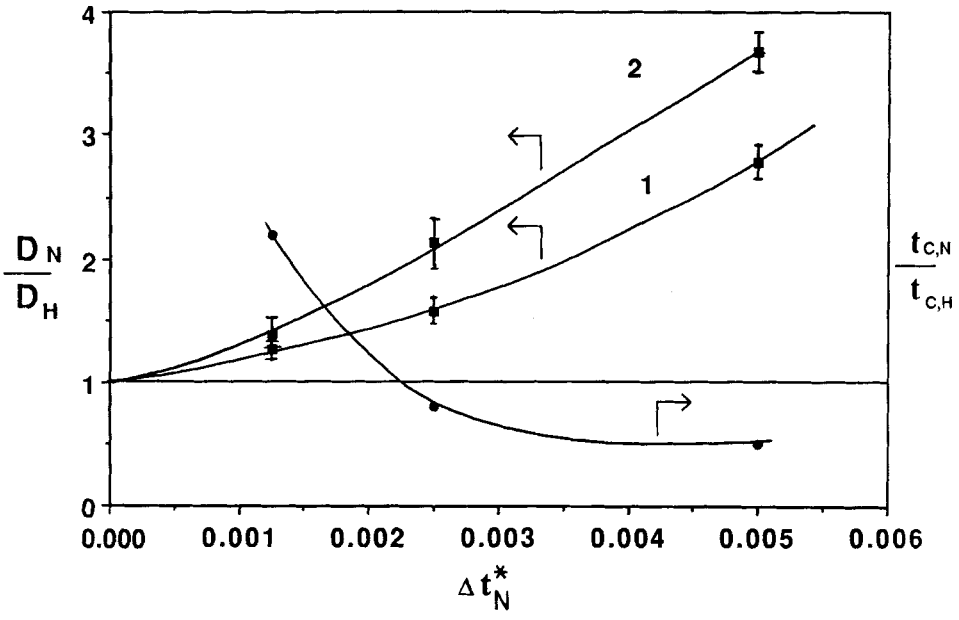

Figure 4 The translational diffusion coefficients, D_N^* and D_H^* obtained from Newton's method and Newton Homotopy Continuation respectively, as a function of the time step, Δt_N^* used in Newton's method. 1: $L^* = 1.0$; 2: $L^* = 2.0$. The CPU time required for the computations involved in these techniques is also shown as a function of Δt_N^*.

of the time step employed in the NR method. Indeed from Figure 4 we observe that the diffusion coefficients obtained from both methods will only coincide in the limit $\Delta t_N^* \to 0$. Moreover, any reduction in the size of the time step used in the NR technique in an attempt to obtain reliable estimates for the diffusion coefficient results in a dramatic increase in the CPU time required. The ratio of the CPU times involved in both methods is plotted in Figure 4 as a function of Δt_N^* and the inability of the NR method to provide reliable results efficiently is clearly demonstrated.

3.2 Translational and rotational motion of the needle within the porous medium

Simulations were conducted over a wide range of needle lengths L^* and porosities ψ to investigate the behavior of the model system. The characteristics of the systems studied and various properties including the collision and free rotational frequencies as well as the frequency of occurrence of glancing collisions relative to tip collisions, are provided in Table 2. In general, it was observed that both the static and dynamic properties displayed different trends at low and high porosities and in the following both regimes will be discussed separately.

At low porosities ($\psi = 0.075$ and $\psi = 0.15$) the VACFs for the small needles exhibit a behavior resembling that of a hard sphere fluid [9] under similar conditions. Figure 5(a) illustrates the VACFs for different needle lengths at a porosity $\psi = 0.15$ and it is observed that for the two smaller needle lengths $L^* = 0.15$ and 0.3, the minimum in the correlation function becomes deeper and shifts to shorter times as the

Table 2 System Characteristics and Selected Properties for the MD Simulations.

ψ	L^*	$^a t^*_{tot}$	$^b \nu_R$	$^c \nu_G/\nu_T$	$^d \nu_c$
0.075	0.1	300	12.05(7)	0.042(1)	6.18(4)
	0.25	300	3.80(4)	0.097(3)	6.29(6)
	0.5	200	0.53(3)	0.215(4)	10.52(8)
	1.0	200	0.060(4)	0.363(6)	8.66(7)
	1.5	150	0.0062(5)	0.581(4)	9.71(4)
	2.0	150	0.00020(3)	0.880(4)	11.55(6)
0.15	0.075	400	17.76(6)	0.0315(1)	4.19(4)
	0.15	400	8.05(4)	0.0638(2)	4.29(7)
	0.3	400	3.19(6)	0.123(3)	4.63(6)
	0.6	200	0.54(6)	0.260(3)	7.19(8)
	1.0	200	0.059(3)	0.361(5)	6.31(7)
	2.0	200	0.003(4)	0.831(4)	8.04(9)
	3.0	250	0.0	1.216(7)	10.27(6)
0.3	1.0	250	0.32(4)	0.397(2)	4.47(3)
	2.0	250	0.023(3)	0.824(1)	4.96(4)
	4.0	250	0.0	1.723(4)	7.72(7)
	6.0	200	0.0	2.49(7)	9.1(1)
0.5	1.0	500	0.54(4)	0.409(5)	2.94(3)
	2.0	500	0.10(2)	0.827(4)	2.92(1)
	4.0	500	0.006(6)	1.623(3)	3.99(3)
	6.0	300	0.0	2.478(3)	5.50(4)
	10.0	250	0.0	4.184(4)	7.34(6)

$^a t^*_{tot}$ is the total time in the trajectory for each configuration, in units of $\sigma\sqrt{m/kT}$.
$^b \nu_R$ is the free rotational frequency in units of $\sqrt{kT/m}/\sigma$.
$^c \nu_G/\nu_T$ is the ratio of the frequency of glancing collisions to that of tip collisions.
$^d \nu_c$ is the average collision frequency in units of $\sqrt{kT/m}/\sigma$.
The average cavity sizes for $\psi = 0.075$ to 0.5 are 0.534, 0.7256, 1.172 and 2.008 respectively in units of σ. Each configuration of the random medium contained 400 solid spheres for all porosities, except $\psi = 0.5$ where 1000 spheres were employed. All results were computed from a statistical sample of 300 configurations.

needle length increases. This trend continues as the particle size increases until the needle length approaches the average size of the cavities within the medium. For a needle length $L^* = 0.6$ the particle experiences severe translational hindrance due tip/sphere chattering collisions and the backscattering minimum in the VACF is at its deepest at this point. This chattering effect is confirmed by the collision frequencies provided in Table 2 which exhibit a local maximum for this needle size.

As the particle size is increased beyond the transition value $L^* = 0.6$ the needle assumes preferred orientations parallel to the solid surface. This is demonstrated in Figure 5(a) where it is observed that the decay in the VACF for the needle length $L^* = 1.0$ is abruptly shifted to longer times. The minima in the VACFs for needle lengths $L^* > 0.6$ are also shallower, indicating that the center of mass experiences weaker backscattering effects due to an increase in the frequency of glancing collisions with needle length as shown in Table 2. However, in addition to the influence of glancing collisions, the coupled effect of tip collisions also exists and it is these collisions which ultimately result in localization of the particle.

At high porosities ($\psi = 0.3$ and $\psi = 0.5$) a transition in the behavior of the VACF is also observed although this transition differs in character from that observed at low porosities. This is illustrated in Figure 5(b) where it is shown that not only are the minima in the VACFs significantly shallower, but also, for a needle length close to the cavity size, the VACF exhibits a forward scattering effect. This positive correlation,

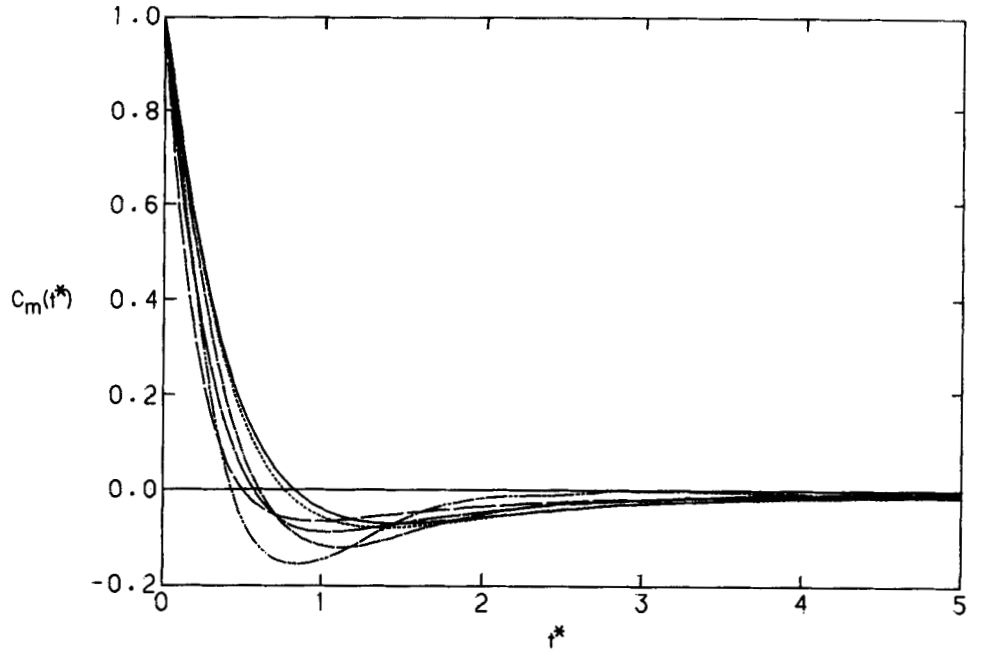

Figure 5(a) The VACFs for the center of mass of the needle as a function of needle length for $\psi = 0.15$. —— $L^* = 0.15$, ···· $L^* = 0.3$, —·— $L^* = 0.6$, ---- $L^* = 1.0$, – – – $L^* = 2.0$, —— $L^* = 3.0$.

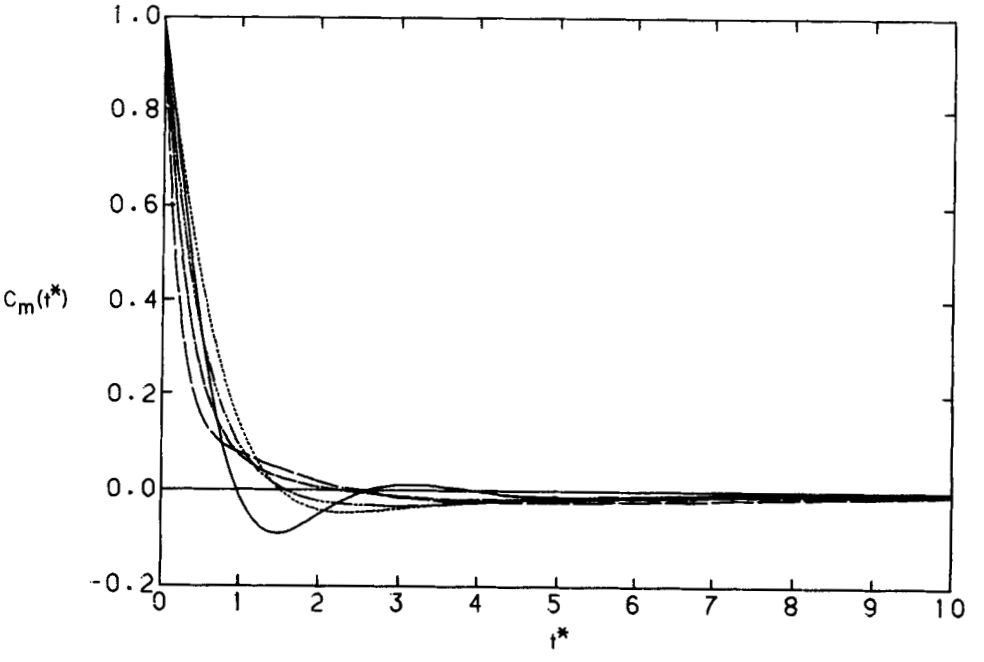

Figure 5(b) The VACFs for the center of mass of the needle as a function of needle length for $\psi = 0.5$. —— $L^* = 1.0$, ···· $L^* = 2.0$, —·— $L^* = 4.0$, – – – $L^* = 6.0$, —— $L^* = 10.0$.

which occurs in this case at the intermediate time $t^* \sim 3.0$, was not detected in the low porosity simulations. Moreover, as will be shown below, the longest needle lengths reported in Table 2 correspond to the translational percolation threshold and it is observed from the free rotational frequencies determined under these conditions that the needles in the high porosity media are also fully hindered rotationally. This latter effect gives rise to an increase in the frequency of glancing collisions which is ultimately responsible for the deceleration in the intermediate-time decay of the VACFs for the long needles.

The general characteristics described above for the center of mass autocorrelation functions are also observed in the directional correlation functions $C_\parallel$ and $C_\perp$. Figures 6(a) and (b) illustrate both of these functions for the range of needle lengths investigated at the porosity $\psi = 0.5$. Comparing Figures 6(a) and (b), we see that for small needle lengths the two functions $C_\parallel$ and $C_\perp$ behave in a similar manner and this is expected when the particle is diffusing isotropically through the medium. For long needles, however, there is a preferential orientation parallel to the solid surface and the particle motion is hindered in the direction perpendicular to its axis. This is clearly indicated by the comparatively slow decorrelation rate of $C_\parallel$ relative to the faster decay rate of $C_\perp$ as the needle length is increased. This effect is further confirmed in the results computed for the correlation function C_u illustrated in Figure 6(c). As may be seen by comparing this figure with Figure 6(a), good agreement between $C_\parallel$ and C_u only exists for long needles when the particle is fully hindered rotationally. However,

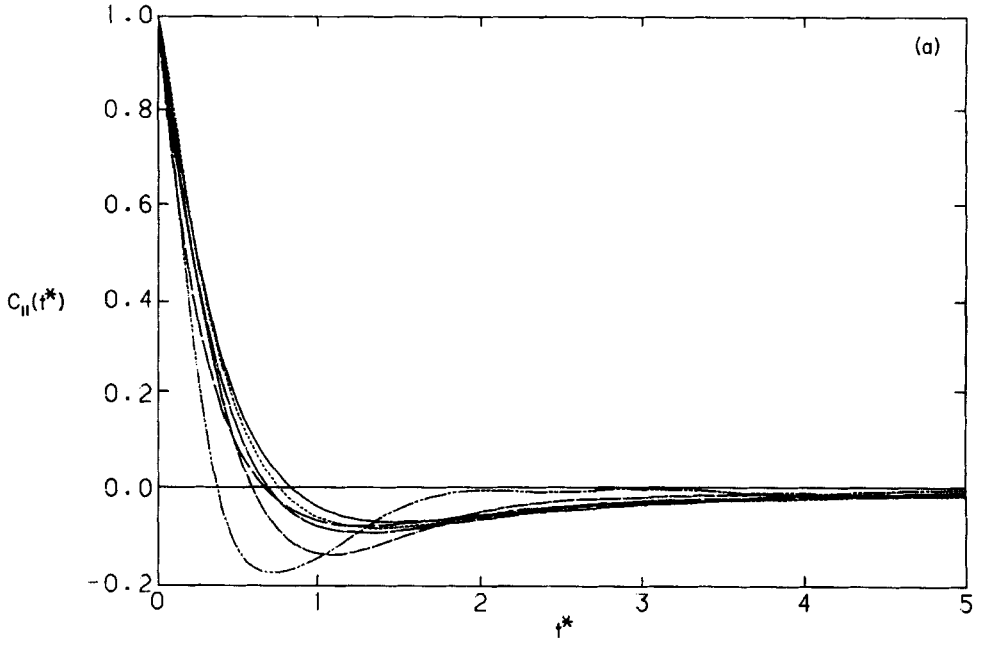

Figure 6 The directional correlation functions as a function of needle for $\psi = 0.5$ (a) $C_\parallel(t^*)$, (b) $C_\perp(t^*)$ and (c) $C_u(t^*)$ where —— $L^* = 0.5$, ····· $L^* = 1.0$, – – – – $L^* = 2.0$, – – – – $L^* = 4.0$, – – – $L^* = 6.0$, —— $L^* = 10.0$.

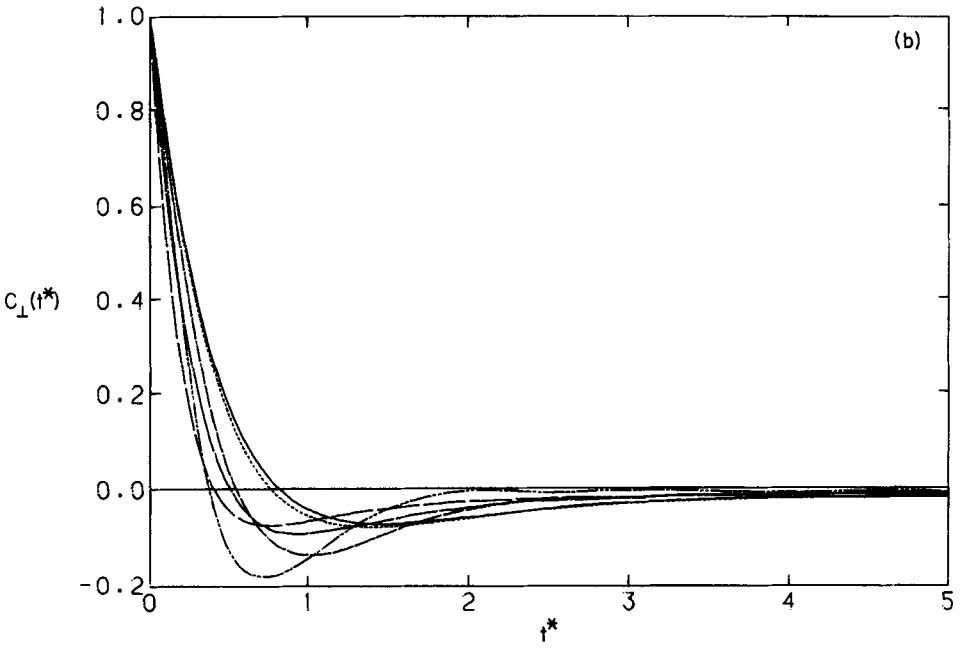

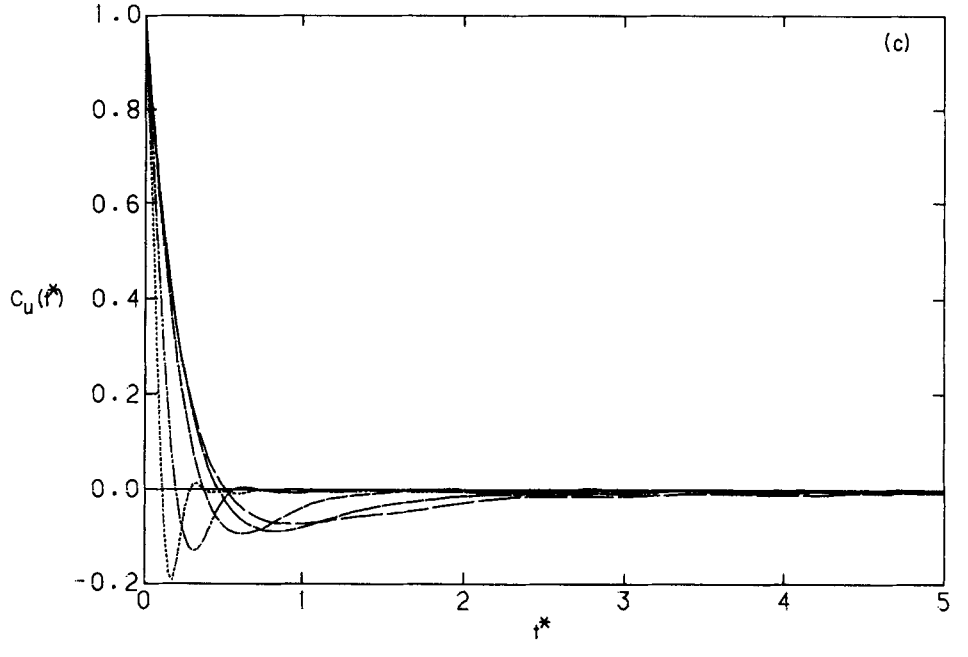

Figure 6 (*continued*)

for very small needles where the orientation vector $\mathbf{u}(t^*)$ is rapidly randomized, there is no similarity between these two functions.

An additional aspect of these correlation functions which is central to an accurate evaluation of the diffusion coefficients of the system, is their behavior at very long times. Theoretical studies of the long-time character of the VACF for a randomly overlapping Lorentz gas [21–26] suggest that the tail of the time-correlation function should decay with an inverse power law given by

$$\lim_{t^* \to \infty} \langle \mathbf{v}(t^*) \cdot \mathbf{v}(0) \rangle = -\frac{\alpha}{t^{*\beta}} \tag{12}$$

This power law implies that the time-dependent diffusion coefficient at long times is also given by

$$\lim_{t^* \to \infty} D^*(t^*) = D^*(t_0^*) + \frac{\alpha}{3(\beta - 1)} [t^{*(1-\beta)} - t_0^{*(1-\beta)}] \tag{13}$$

The statistical accuracy of the tails of the VACFs computed here was insufficient to provide reliable estimates of α and β from a fit of Equation (12) however satisfactory results for these parameters were obtained from nonlinear regression of the integrated form provided in Equation (13). In this estimation procedure, the time t_0^* in Equation (13) was typically chosen to be $\sim 10\, t_{\min}^*$ where $t_{\min}^*$ corresponds to the time at which the minimum in the VACF occurs. The results obtained are provided in Table 3 and as indicated in this table, in a few cases it was not possible to determine the parameters

Table 3 Parameters for the Long-Time Tail of the VACF.

ψ	L^*	[a]α	[b]β
0.075	0.1	0.305(4)	1.68(2)
	0.25	0.167(5)	1.52(2)
	0.5	-	-
	1.0	0.093(3)	1.85(1)
	1.5	0.072(6)	1.65(2)
	2.0	0.004(3)	1.5(1)
0.15	0.075	0.41(1)	1.69(4)
	0.15	0.17(5)	1.40(2)
	0.3	0.216(7)	1.37(5)
	0.6	-	-
	1.0	0.42(3)	1.98(4)
	2.0	0.172(8)	1.51(2)
	3.0	0.102(4)	1.4(1)
0.3	1.0	-	-
	2.0	1.4(1)	2.1(2)
	4.0	1.27(3)	2.1(1)
	6.0	0.22(2)	1.4(2)
0.5	1.0	-	-
	2.0	-	-
	4.0	-	-
	6.0	0.56(1)	1.7(1)
	10.0	0.68(9)	1.4(2)

[a] α is the units of $(m/kT)^{\beta/2}\sigma^{\beta-2}$.
[b] β was estimated by nonlinear regression of Equation (13).

α and β due to rapid decorrelation of the particle velocity. This is particularly noticeable in the transition region between free and hindered rotation.

The theoretical value of the power-law exponent β in Equations (12) and (13) is 2.5 in the hydrodynamic limit for structureless particles in random media [25, 26] and earlier studies reported in [9, 27] confirmed this prediction. In our model system the hydrodynamic limit will only apply for very small needles in high porosity media and as seen in Table 3, the parameter β for the smallest needle investigated here is significantly below the value 2.5. We believe that this is due to partial exclusion of the needle from regions of the pore space, even in high porosity systems, and the topological constraints imposed by this exclusion effect result in the appearance of anomalous behavior in the particle dynamics. Moreover, as the length of the needle is increased the exponent β decreases until the needle size approaches the size of the average cavities within the medium. As indicated in Figures 5(a) and (b) the tails of the time-correlation functions in this transition region decay rapidly to zero, implying the existence of a comparatively large power-law exponent under these conditions. This is clearly demonstrated by the β values obtained for the needle length $L^* = 1.0$ in the two low porosity runs provided in Table 3. For longer needles the exponent β decreases again until the percolation threshold for that porosity is reached. At the percolation threshold the values of β in Table 3 for each case are, within the statistical accuracy of the data, equal to 1.4. This result is consistently lower than the value of 1.57 reported in [9] for the percolation transition of a point particle in the random overlapping spheres medium. This strongly suggests that the power-law exponent β is not a universal constant for a given random medium and is affected by the shape of the diffusing particle. Furthermore, since $C_\parallel$ and $C_\perp$ are correlation functions of the components of the center of mass velocity, we expect these functions to exhibit a similar time-dependent character and this was indeed found to be the case. The β values obtained from nonlinear regression of the time-dependent diffusion coefficients $D_\parallel^*(t^*)$ and $D_\perp^*(t^*)$ using Equation (13), were found to be consistent with those reported in Table 3.

The infinite time diffusion coefficients D_m^*, $D_\parallel^*$ and $D_\perp^*$ obtained by extrapolating the data using Equation (13) are provided in Table 4. The translational diffusion coefficient D_m^* is plotted as a function of needle length in Figure 7. The trends observed in this figure are primarily related to the effects of needle alignment within the pores and the void space available for diffusion. For each of the porosities investigated, the diffusion coefficient D_m^* is a nonmonotonic function of L^* exhibiting both a minimum and a maximum as the particle size is increased. The minimum corresponds to a particle size approaching that of the average cavities in the medium and arises primarily due to chattering collisions between the needle and the solid spheres. This behavior was also noted earlier with regard to the deep minima in the VACFs at the transition point shown in Figures 5(a) and (b). As L^* is increased further the needle is predisposed to align itself parallel to the solid surface and the diffusion rate is enhanced due to partial specular scattering during glancing collisions. At a particular length, however, this effect is diminished due to restricted availability of the void space within the porous medium and D_m^* passes through a maximum. For very long needles, localization sets in and D_m^* rapidly approaches zero. As expected, the percolation threshold of the medium shifts to longer needle sizes as the porosity increases.

For comparative purposes, in Figure 7 we also illustrate the diffusivities reported earlier for a hard-sphere fluid in a random overlapping spheres medium [9]. The length scale employed here to construct these plots corresponds to the diameter of the

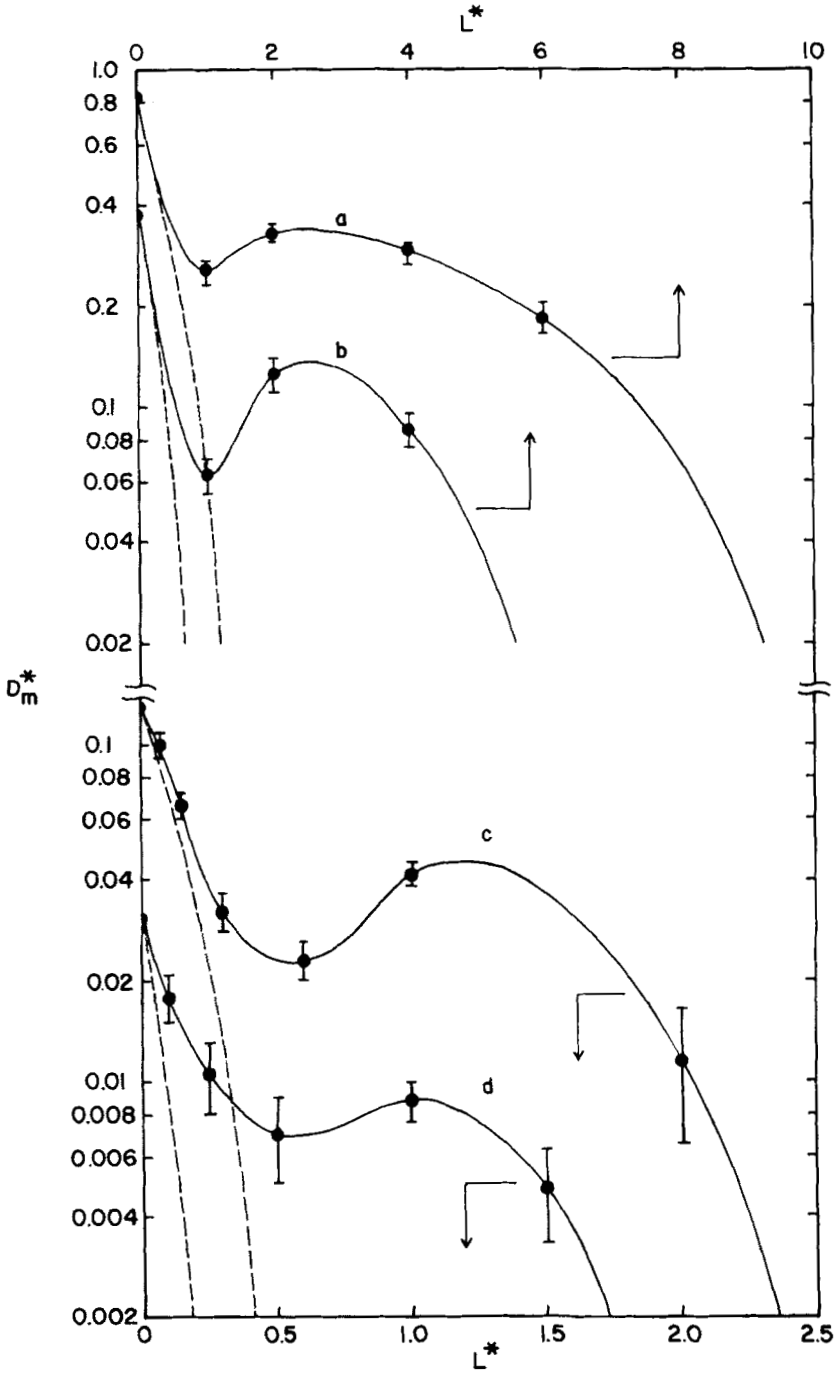

Figure 7 The translational diffusion coefficient as a function of needle length. (a) $\psi = 0.5$, (b) $\psi = 0.3$, (c) $\psi = 0.15$, (d) $\psi = 0.075$. The dashed lines in each case correspond to the results for a hard sphere fluid diffusing through the random medium, where the diameter of the sphere is equal to L^*.

Table 4 Diffusion coefficients as functions of L^* and ψ

ψ	L^*	$^aD_m^*$	$^aD_\parallel^*$	$^aD_\perp^*$	$^bD_r^*$
0.075	0.1	0.018(3)	0.016(4)	0.017(3)	0.53(2)
	0.25	0.011(3)	0.021(4)	0.005(2)	0.44(2)
	0.5	0.007(2)	0.010(2)	0.005(4)	0.139(6)
	1.0	0.009(2)	0.022(2)	0.0018(5)	0.117(5)
	1.5	0.005(2)	0.010(3)	0.0002(3)	0.067(3)
	2.0	0.0	0.0	0.0	0.043(2)
0.15	0.075	0.101(5)	0.110(4)	0.115(5)	0.79(3)
	0.15	0.066(5)	0.112(5)	0.050(5)	0.75(3)
	0.3	0.032(4)	0.029(2)	0.028(2)	0.57(2)
	0.6	0.023(3)	0.017(3)	0.026(3)	0.201(9)
	1.0	0.041(3)	0.048(5)	0.039(3)	0.21(2)
	2.0	0.011(5)	0.025(2)	0.0064(7)	0.085(4)
	3.0	0.0	0.0	0.0	0.035(2)
0.3	1.0	0.063(7)	0.093(6)	0.048(6)	0.31(1)
	2.0	0.119(5)	0.113(3)	0.123(2)	0.196(8)
	4.0	0.085(3)	0.179(6)	0.040(3)	0.068(3)
	6.0	0.0	0.0	0.0	0.021(2)
0.5	1.0	0.26(2)	0.28(2)	0.25(2)	0.65(2)
	2.0	0.33(2)	0.42(1)	0.29(9)	0.42(1)
	4.0	0.28(1)	0.39(4)	0.16(6)	0.196(5)
	6.0	0.18(1)	0.46(2)	0.049(4)	0.102(2)
	10.0	0.0	0.0	0.0	0.025(1)

$^aD_m^*$, $D_\parallel^*$ and $D_\perp^*$ are in units of $\sigma\sqrt{kT/m}$.
$^bD_r^*$ is in units of $\sqrt{kT/m}/(I\sigma)$ where I is the moment of inertia of the needle.

diffusing hard-sphere particle and it is clearly seen from this figure that the percolation transition in this case occurs for much smaller particle sizes. The severe hindrance effects indicated here for spherical particles in comparison with the needle fluid should have a direct bearing on the relative permselectivity of iinear and branched chain molecular fluids in microporous media.

Further evidence of the influence of particle alignment is provided by the diffusion coefficients $D_\parallel^*$ amd $D_\perp^*$. These two coefficients combine to give the overall translational diffusivity D_m^*

$$D_m^* = \frac{D_\parallel^* + 2D_\parallel^*}{3} \tag{14}$$

as may be seen using the results given in Table 4. For small needles, we observe near equality of $D_\parallel^*$ and $D_\perp^*$ since the diffusion process is isotropic. However, there is a change in trend with increasing particle size which lowers the value of $D_\perp^*$ due to hindered diffusion of the needle perpendicular to its axis. This is also confirmed by the fact that $D_\parallel^*$ approaches $3D_m^*$ as the needle length increases and for very long needles the diffusion process is primarily controlled by motion along the axis of the particle.

The conclusions provided above for the behavior of D_m^* are confirmed by the RDFs shown in Figures 8 and 9. These RDFs were obtained by a straightforward Monte Carlo insertion technique and were found to be in agreement with those computed by MD simulation. Furthermore, in support of the reliability of the simulation procedures employed here, it was found that the partition coefficients K determined in the

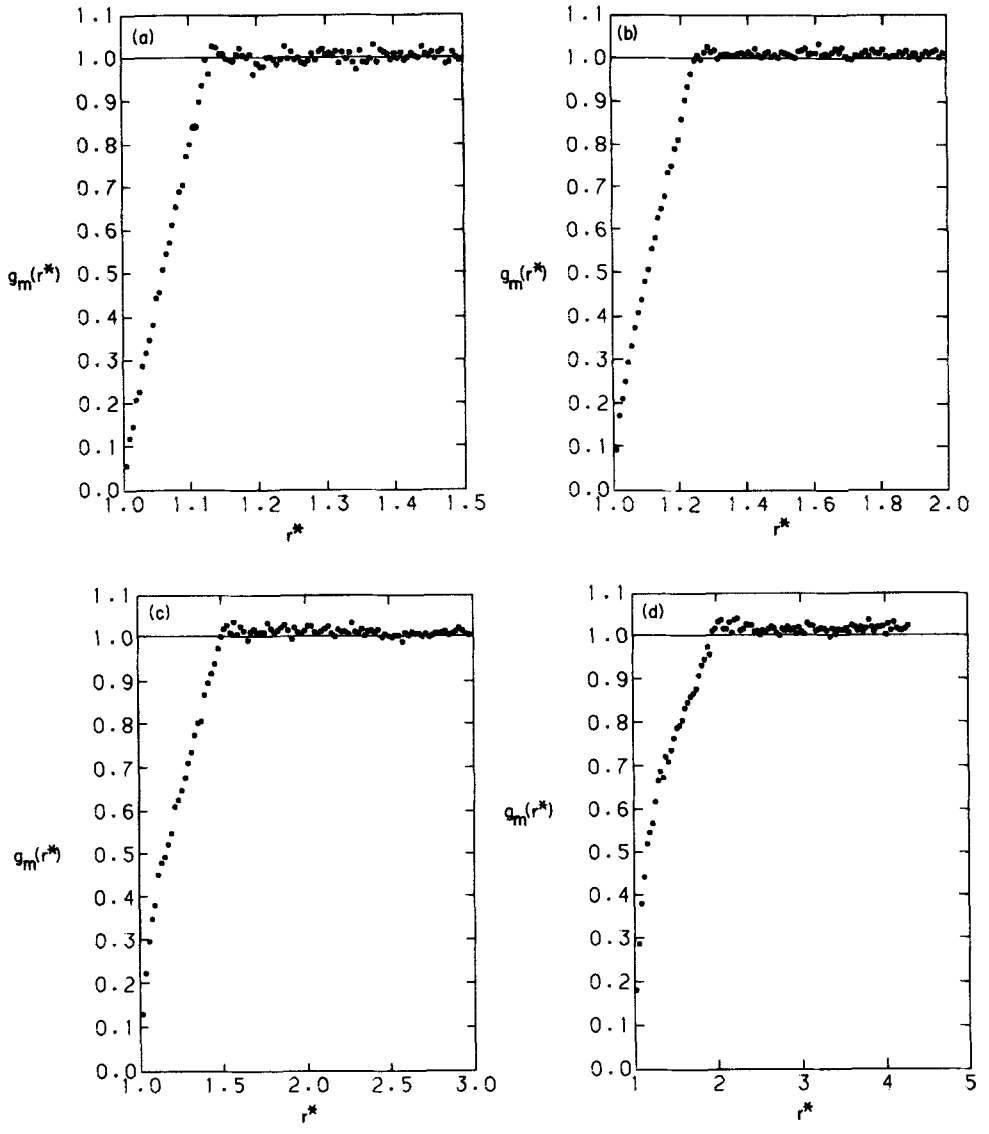

Figure 8 The radial distribution functions for the center of mass of the needle for $\psi = 0.075$. (a) $L^* = 0.25$, (b) $L^* = 0.5$, (c) $L^* = 1.0$, (d) $L^* = 2.0$.

MC simulations were also in excellent agreement with the theoretical expression

$$K = \psi^{(1+\frac{1}{2}L^*)} \tag{15}$$

The contact value for the center of mass RDFs is zero while it is 0.5 for the tip distribution functions. The latter result arises because the distribution of solid spheres in contact with the needle tip is confined to a hemispherical surface. Moreover, for small needles we expect the RDFs to be equal to 1.0 at a relative separation $r^* = L^*/2$

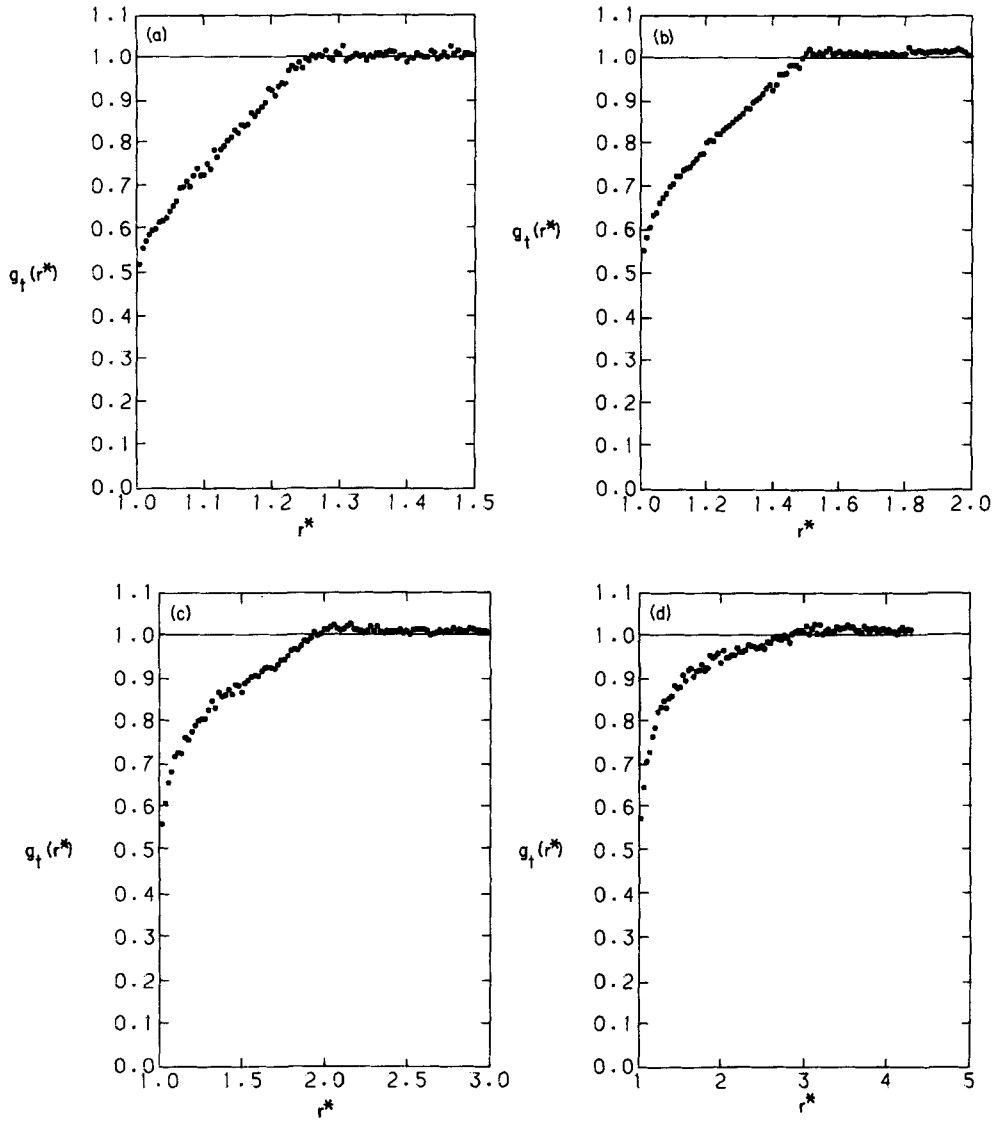

Figure 9 The radial distribution functions for the tips of the needle for $\psi = 0.075$. (a) $L^* = 0.25$, (b) $L^* = 0.5$, (c) $L^* = 1.0$, (d) $L^* = 2.0$.

for the center of mass RDFs and $r^* = L^*$ for the tip RDFs. Figures 8(a) and 9(a) illustrate this feature for a needle length $L^* = 0.25$ at a porosity $\psi = 0.075$. As the needle length is increased (see Figures 8(c) and (d)), the RDFs tend to approach 1.0 for shorter interparticle separations indicating that the needle is not randomly oriented but is preferentially inclined to the solid surface. Another interesting aspect which also confirms needle alignment is the increasing convexity of the RDF in the vicinity of the contact point as the needle length increases, while for very small needles the distribution function is linear in this region. Furthermore, for long needles, the RDFs

are consistently larger than 1.0 for interparticle separations greater than $L^*/2$ (or L^*). We believe that the latter effect arises due to the higher than average local density of the solid spheres surrounding a cavity which is sufficiently large to accomodate the longest needles employed in the simulations.

The remaining properties investigated here are associated with the rotational motion of the needle which is characterized by the angular velocity autocorrelation function (RACF) defined in Equation (5). Figure 10 illustrates the RACFs for different needle lengths at a porosity $\psi = 0.15$. These time-correlation functions also display the effect of needle alignment when its size is larger than that of the average pore diameter. From this figure, it is further observed that in the transition region at $L^* = 0.6$, the decay rate of the time-correlation function significantly increases indicating that the rotation of the particle is strongly influenced by the chattering collisions discussed earlier. Longer needles display similar decay processes as well as significant backscattering effects which become more pronounced as the needle length increases. It is also noteworthy in this respect that long-time tails in the RACFs were found to be nonexistent within the accuracy of the data. For this reason, the integration of the time-correlation functions to determine the rotational diffusion coefficient did not require extrapolation beyond the range of the simulation data.

The rotational diffusion coefficients D_r^* obtained by integrating the RACFs are provided in Table 4 and are shown in Figures 11(a) and (b). For both high and low porosities, it is seen that D_r^* passes through a transition region as the needle length is increased and the size of the particle at which this transition occurs corresponds to the needle length at which the minimum in D_m^* was observed earlier. This transition is particularly evident at low porosities where it is also observed that the rotational

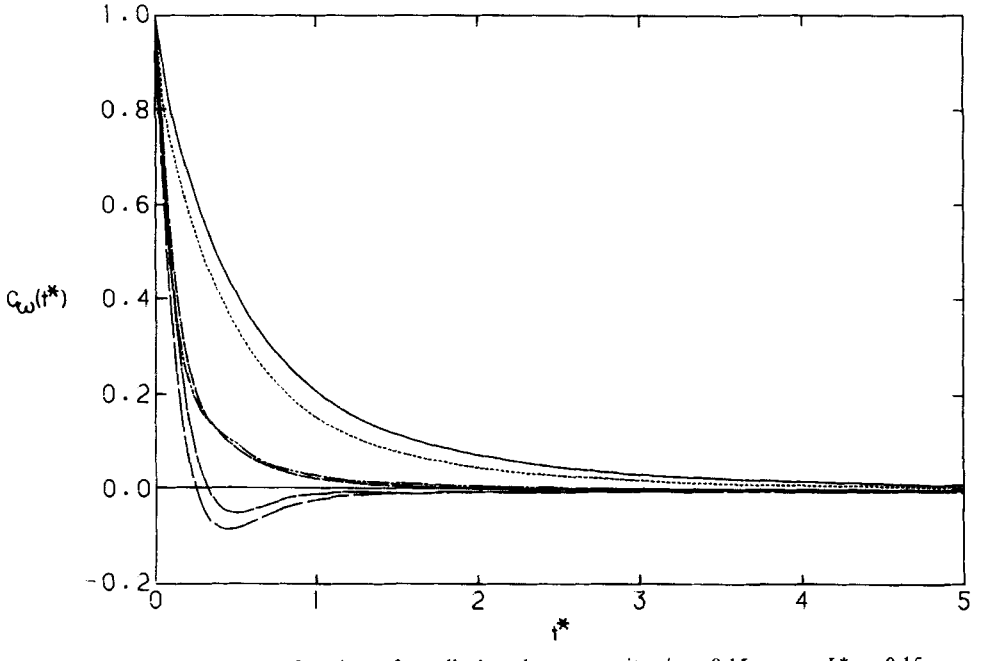

Figure 10 The RACF as a function of needle length at porosity $\psi = 0.15$ —— $L^* = 0.15$, ···· $L^* = 0.3$, —·— $L^* = 0.6$, - - - - $L^* = 1.0$, – – – $L^* = 2.0$, —— $L^* = 3.0$.

diffusion coefficient is a nonmonotic function of L^*. For needle lengths less than 1.0 the very sharp drop in D_r^* is directly related to the rapid decrease in the free rotational frequency, ν_R, shown in Table 2 over the same range of particle sizes. However, for the longest needles studied, D_r^* varies exponentially with needle length and this behavior was generally found irrespective of the porosity of the medium.

4 SUMMARY AND CONCLUSIONS

In this paper we have investigated the dynamics of a dilute needle fluid diffusing through a random overlapping spheres model of a porous medium. Although this model is rather simple, the needle/sphere collision sequence is not reliably handled by traditional collision tracking algorithms and we have employed a new technique known as Newton Homotopy Continuation to overcome this difficulty. The NHC algorithm is particularly attractive due to its robustness and it has been demonstrated that it is not subject to the problems of root bypassing which are prominent in the Newton–Raphson method. Furthermore, the homotopy continuation method is quite versatile and may be adapted to other hard body fluids. We are currently investigating

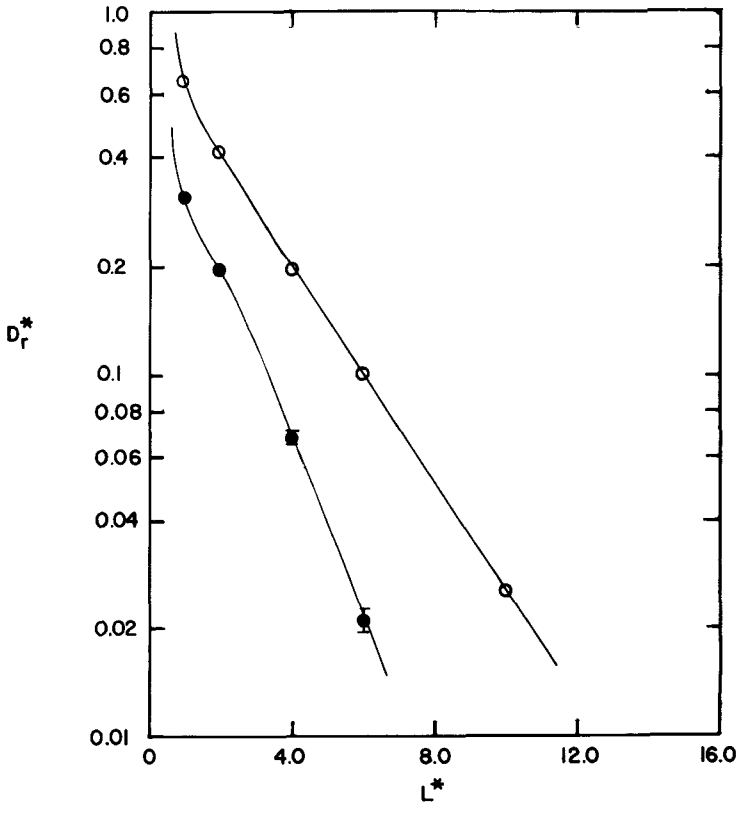

Figure 11(a) The rotational diffusion coefficient as function of L^*. ○ $\psi = 0.5$, ● $\psi = 0.3$.

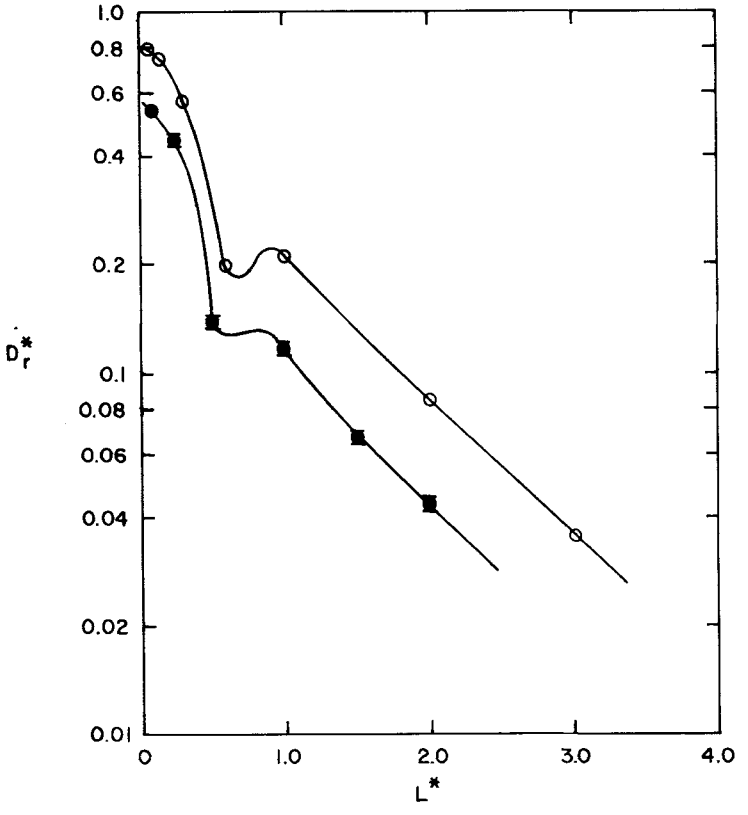

Figure 11(b) The rotational diffusion coefficient as a function of needle length. ○ $\psi = 0.15$, ● $\psi = 0.075$.

this possibility for other systems including bulk homogeneous fluids as well as confined fluids in micropores.

The MD simulations conducted in this work have also provided a number of interesting results related to the influence of particle asphericity on diffusion within a random medium. One of the most important aspects of these results was with regard to the trend observed in the translational diffusion coefficient D_m^* of the needle particle as function of its length. Enhanced diffusivities were observed as the needle length was increased and we associate this with needle alignment parallel to the solid surface arising from the rotational hindrance it experiences within the pores. Comparison with earlier results reported for spherical particle simulations also suggests that the random medium is selectively permeable to linear molecular structures and this type of selectivity should play an important role in separation processes involving particles of different size and structure. Shape selectivity has long been recognized for crystalline media such as molecular sieve zeolites and the results reported here support the view that this behavior may also be a dominant factor in microporous amorphous media. Although the hard-body model investigated in this paper is highly idealized, in future work we intend to ascertain the relative importance of this selectivity mechanism for more realistic aspherical particles by relaxing the constraint of particle

linearity and by introducing soft potentials and forces for the intermolecular interactions.

Acknowledgements
We gratefully appreciate the many helpful discussions with Dr. S. Choi concerning the NHC technique and its applications.

APPENDIX

A brief description of the Newton Homotopy procedure and the path tracking method is provided here. The homotopy function for NHC is defined by Equation (3) in the text. The path is the locus of the points for which the function $h(t, \tau) = 0$ and is traced from a starting point on the $\tau = 0$ hyperplane using a predictor-corrector technique.

The predictor employed in the path tracking method is a first order Euler predictor which is defined by the unit tangent $\mathbf{u}_t^k$ at the kth point times the step size Δs_k

$$\mathbf{w}_p^{k+1} = \mathbf{w}^k + \mathbf{u}_t^k \Delta s_k \tag{A1}$$

where $\mathbf{w}_p^{k+1}$ is the $k+1$th point on the path predicted by an Euler predictor and $\mathbf{w}^k$ is the previous point. If this new point is not in the domain of $h(t,\tau)$ then the step size is halved.

After the initial prediction, the point is then corrected on to the homotopy path using a Newton corrector given by following set of equations

$$\left.\frac{\partial \mathbf{h}}{\partial \mathbf{w}}\right|_k \Delta \mathbf{w}^{k+1} = -\mathbf{h}^k \tag{A2}$$

$$(\mathbf{u}^k)^T \Delta \mathbf{w}^{k+1} = 0 \tag{A3}$$

where $\Delta \mathbf{w}^{k+1}$ is the Newton corrector. The vector notation for the homotopy function $\mathbf{h}$ is used here to emphasise the importance of the directionality of the path. The new corrected point is given by

$$\mathbf{w}_c^{k+1} = \mathbf{w}^k + \Delta \mathbf{w}^{k+1} \tag{A4}$$

This correction procedure is carried out iteratively until the following condition is satisfied [28]

$$\|\mathbf{h}^{k+1}\| < \varepsilon_{cor} \|\partial \mathbf{h}/\partial \mathbf{w}\| \tag{A5}$$

where $\partial \mathbf{h}/\partial \mathbf{w}$ is evaluated at the predicted point $\mathbf{w}_p^{k+1}$ and ε_{cor} is a small positive number. The $\|\cdot\|$ represent the Euclidean norm of the quantity enclosed. Moreover, to reduce the number of iterations required for the correction step, the size of step in the prediction routine is kept sufficiently small. It is important to note that the error associated with the new point is not affected by the history of the homotopy path and hence the tolerance on the correction step need not be very high. The path is then continuously tracked by repeating this predictor-corrector procedure until the path intersects the $\tau = 1$ hyperplane or diverges to infinity.

Furthermore, to adapt the path tracking algorithm developed by Choi [19] to our model system, we have made modifications regarding the stopping rules and other conditions needed to discontinue the root search. If the condition

$(1 - \tau^k)(1 - \tau^{k+1}) < 0$ is satisfied, then there are an odd number of roots between the two points k and $k+1$. A bisection search is then carried out until $\Delta s^k < \varepsilon_{sol} \|\mathbf{w}^{k+1}\|$ where ε_{sol} is a tolerance on the Euclidean norm of the tangent at the present point $k+1$ given by $\|\mathbf{w}^{k+1}\|$ and Δs^k is the step size. The path tracking procedure is stopped if any of the following conditions are met

(a) $t^k < t^{k+1}, \quad t^k, t^{k+1} > 0$
(b) $t^k > t^{k+1}, \quad t^k, t^{k+1} < 0$
(c) $t^{k+1} < 0, \quad t^k > 0$

where t^k and t^{k+1} are two roots on the same homotopy path obtained at the intersection with the $\tau = 1.0$ hyperplane. These rules apply regardless of whether the path has been tracked from the positive or negative directions of τ. The step size used here should not be confused with the time step used in the NR method. In the homotopy continuation technique the step Δs_k is used to track the homotopy path and not the actual function. Moreover, the magnitude of the homotopy step size is of the order of 10^{-6} which is much smaller than the typical time step used in the NR method.

If the particle does not collide with a solid sphere the homotopy path goes to infinity and this is detected by the condition $\|\mathbf{w}^{k+1}\| > M$, where M is a large positive number which in our system is of the order of 10^5. Moreover, when the path does not intersect the $\tau = 1$ hyperplane and the condition $\|\mathbf{w}^{k+1}\| > \|\mathbf{w}^k\|$ is satisfied, this implies that the path is exhibiting asymptotic behavior. This is observed by counting the number of successive steps on the homotopy path satisfying the condition

$$\left\| \frac{d}{ds} \mathbf{w}^{k+1} - \frac{d}{ds} \mathbf{w}^k \right\| < \varepsilon_{asym} \tag{A6}$$

where ε_{asym} is a small positive number which in our case is given by $\varepsilon_{asym} = 10^{-6}$. When the count is greater than five the path is assumed to be asymptotic to the $\tau = 1$ hyperplane and as the count reaches twenty the path is assumed to diverge to infinity. Under these conditions the continuation procedure is terminated. These modifications are particularly unique to our system and a careful analysis is required to adapt this procedure to other systems.

References

[1] B.J. Alder and T.E. Wainwright, "Studies in Molecular Dynamics. II. Behavior of a Small Number of Elastic Spheres", *Phys. Rev.* A, **1**, 18 (1970).

[2] J. Talbot, M.P. Allen, G.T. Evans, D. Frenkel, and D. Kivelson, "Accuracy of Enskog Theory for Rotational versus Translational Motion – a Molecular Dynamics Study", *Phys. Rev. A*, **39**, 4330, (1989).

[3] K.M. Sando and D.W. Rebertus, "Molecular Dynamics Simulations of a Fluid of Hard Spherocylinders", *J. Chem. Phys.*, **67**, 2585 (1977).

[4] D. Frenkel and J.F. Maguire, "Molecular Dynamics Study of the Dynamical Properties of an Assembly of Infinitely Thin Hard Rods", *Mol Phys.*, **49**, 503 (1983).

[5] J.J. Magda, H.T. Davis and M. Tirrell, "The Transport Properties of Rod-like Particles via Molecular Dynamics. I. Bulk Simulation.", *J. Chem. Phys.*, **85**, 6674 (1985).

[6] M.P. Allen and I.C.H. Cunningham, "A Computer Simulation Study of Idealized Model Tetrahedral Molecules", *Mol. Phys.*, **58**, 615 (1986).

[7] M.P. Allen and A.A. Imbierski, "A Molecular Dynamics Study of a Hard Dumb-bell System", *Mol. Phys.*, **60**, 453 (1987).

[8] G.A. Chapela, S.E. Martinez-Casas, and J. Alejandre, "Molecular Dynamics for Discontinuous Potentials. I. General method and Simulation of Hard Polyatomic Molecules", *Mol. Phys.* **53**, 139 (1984).

[9] I.-A. Park and J.M.D. MacElroy, "Simulation of a Hard-Sphere Fluid in Bicontinuous Random Media", *Mol. Sim.*, **2**, 105 (1989).
[10] L.A. Fanti and E.D. Glandt, "Partitioning of Spherical Particles into Fibrous Matrices", *J. Coll. I. Sci.*, **135**, 385 (1990); *J. Coll. I. Sci.*, **135**, 396 (1990).
[11] L.A. Fanti and E.D. Glandt, "Partitioning of Spherical Solutes into Sponge-type Material" *AIChE J.*, **35**, 1883 (1989).
[12] C.K. Hall and R. Dickman, "High Density Monte Carlo Simulations of Chain Molecules. Bulk Equation of State and Density Profiles near Walls", *J. Chem. Phys.*, **89**, 3168 (1988).
[13] A. Yethiraj and C.K. Hall, "Monte Carlo Simulations of Hard Chain – Hard Sphere Mixtures in Slit-like Pores" *J. Chem. Phys.*, **91**, 4827 (1989).
[14] J.J. Magda, M. Tirrell and H.T. Davis, "The Transport Properties of Rod-like Particles. II. Narrow Slit Pore", *J. Chem. Phys.*, **88**, 1207 (1988).
[15] I. Bitsanis and G. Hadziioannou, "Molecular Dynamics Simulations of the Structure and Dynamics of Confined Polymer Melts", *J. Chem. Phys.*, **92** 3827 (1990).
[16] H.L. Weissberg, "Effective Diffusion Coefficients in Porous Media", *J. Appl. Phys.*, **34**, 2636 (1963).
[17] J.D. Seader, *Recent Developments in Methods for finding all Solutions to General System of Non-linear Equations*, Conference on Foundation of Computer-Aided Process Design, July 1989, Snowmass, CO.
[18] T.L. Wayburn, "A Review of Continuation Methods and Their Application to Separation Problems", *Comp. and Tech. Div. Comm.*, **11**, 8 (1988).
[19] S.H. Choi, *The Applications of Global Homotopy Continuation Methods to Chemical Process Flowsheeting Problems*, Ph.D dissertation, Dept. of Chem. Engr., Univ. of Missouri-Rolla (1990).
[20] B.J. Berne, "Time-Dependent Properties of Condensed Media", Ch. 9 in *Physical Chemistry – An Advanced Treatise*, Vol 8B, D. Henderson (Ed.), Academic Press, N.Y. (1971).
[21] T. Keyes and J. Mercer, "Some Considerations on the Calculation of the Velocity Correlation Function in the Ring Approximation, with Application to the Lorentz Gas", *Physica*, **95A**, 473 (1979).
[22] W. Gotze, E. Leutheusser, and S. Yip, "Dynamical Theory of Diffusion and Localization in a Random, Static Field", *Phys. Rev. A*, **23**, 2634 (1981).
[23] W. Gotze, E. Leutheusser and S. Yip, "Correlation Functions for the Hard-Sphere Lorentz Model", *Phys. Rev. A*, **24**, 1008 (1981).
[24] A. Masters and T. Keyes, "Diffusion, Percolation and Trapping in the Lorentz Gas via Variational Kinetic Theory", *Phys. Rev. A*, **26**, 2129 (1982).
[25] M.H. Ernst, J. Machta, J.R. Dorfman, and H. van Beijeren, "Long-Time Tails in Stationary Random Media. I. Theory", *J. Stat. Phys.*, **34**, 477 (1984).
[26] J. Machta, M.H. Ernst, H. van Beijeren, and J.R. Dorfman, "Long-Time Tails in Stationary Random Media. II. Applications", *J. Stat. Phys.*, **35**, 413 (1984).
[27] J.M.D. MacElroy and K. Raghavan, "Adsorption and Diffusion of a Lennard-Jones Vapor in Microporous Silica", *J. Chem. Phys.*, **93**, 2068 (1990).
[28] E.L. Allgower and K. Georg, "Simplicial and Continuation Methods for Approximating Fixed Points and Solutions to System of Equations", *SIAM Review*, **22**, 28 (1980).